Journal of Structural and Construction Engineering

www.jsce.ir

# Numerical Investigation of the Hysteretic Behavior of Steel Plate Shear Walls with Corner Openings Considering Steel Damage

**Inas Jasim Kadhim[1], Mohammad Reza Sheidaii[2]***

*1- PhD Student, Engineering Faculty, Urmia University, Urmia, Iran*
*2- Professor, Engineering Faculty, Urmia University, Urmia, Iran*

## ABSTRACT

*The widespread use of steel plate shear walls (SPSWs) in structures designed to withstand lateral forces, especially during seismic events, has gained significant traction due to their high load-bearing capacity and efficient energy dissipation capabilities. Previous studies have highlighted the significant influence of wall openings on the load-bearing characteristics of SPSWs. This study employs a detailed numerical approach using the finite element method to investigate the effects of corner openings on the performance of SPSWs. Twenty-seven numerical models were developed, incorporating variables such as plate thickness, the horizontal corner opening percentage (the size of corner openings along the horizontal direction, expressed as a percentage of the total boundary element length), and the opening aspect ratio (horizontal to vertical dimensions of the openings). These models were analyzed using ABAQUS, and nonlinear dynamic analysis was conducted to evaluate their performance. The results indicate that the degree and configuration of openings play a decisive role in the seismic performance of SPSWs. While larger openings reduce lateral strength, stiffness, and energy dissipation, unequal openings of up to 10% achieve an optimal balance - effectively decreasing force demand without noticeably compromising performance. Plate slenderness showed minimal influence on failure behavior, confirming that the optimal design depends primarily on the controlled level of discontinuity rather than plate thickness.*

## ARTICLE INFO

**Receive Date:** 30 June 2025
**Revise Date:** 18 October 2025
**Accept Date:** 28 November 2025

**Keywords:**
*Steel plate shear wall*
*corner discontinuity*
*cyclic curves*
*bearing capacity*
*non-linearity of materials*



**doi:** 10.22065/jsce.2025.528037.3753

*Corresponding author: Mohammad Reza Sheidaii
Email address: m.sheidaii@urmia.ac.ir

# 1- Introduction

In recent years, steel plate shear walls (SPSWs) have become widely recognized as an efficient lateral load-resisting system. An SPSW consists of vertical and horizontal boundary elements and a thin infill steel plate that contributes significantly to lateral strength and stiffness through the development of tension-field action. This system offers high elastic stiffness, ductility, and energy dissipation capacity, leading to stable cyclic performance. Compared with concrete walls, SPSWs are lighter and more space-efficient, providing architectural advantages.

However, the thin plate -often thicker in practice due to welding requirements- buckles easily under shear, relying on post-buckling tension fields for strength. The boundary elements restrain this field and thus experience considerable force demands, which may increase the structural weight or cause premature failure. Furthermore, architectural openings disturb the tension-field mechanism, reducing stability. To address these issues, researchers have proposed strategies such as partial disconnection of boundary elements, introducing openings or slits, and using mild steel plates to control stiffness and boundary forces.

In SPSWs, vertical boundary elements are connected to the wall plate on one side, forcing the entire tension field to transfer through them and often requiring heavier sections. Introducing localized disconnections between the plate and boundary elements may therefore be more beneficial than adding openings. This study numerically investigates the effects of corner opening size and ratio on cyclic behavior, tension-field development, and the required strength of vertical boundary elements.

Numerous studies have investigated the behavior of steel plate shear walls (SPSWs), highlighting that in conventional systems, the post-buckling behavior of the infill plates induces significant stresses on the vertical boundary elements (VBEs). To prevent plastic deformations in the columns that may compromise structural integrity, robust columns are essential. Addressing these challenges, researchers have proposed various mitigation strategies, such as introducing wall openings and partially disconnecting infill plates from adjacent VBEs, to reduce the force demands on boundary members. A key challenge in selecting appropriate SPSW systems lies in determining whether the infill panel at a given location should be strengthened by increasing its thickness and yield strength. Such modifications often require larger and stronger vertical and horizontal boundary elements, as their design is generally governed by the capacity of the infill plate.

To mitigate this issue, recent research has concentrated on the use of light-gauge steel [1], low-yield steel (LYS) plates [2,3], and perforated patterns to reduce panel strength and stiffness [2,4,5]. Furthermore, the investigation of reduced beam sections as horizontal boundary members has been conducted to alleviate the overall demand on the vertical members within the system [2,4,5]. Purba and Bruneau [6] developed finite element models using shell elements to analyze perforated steel plate shear walls. Their study employed a simplified diagonal strip model, revealing two key findings: (1) individual strips behave independently without stress-transfer interactions, and (2) finite element analysis yields accurate predictions when hole diameters are maintained below 60% of strip width.

Moghimi and Driver [7] conducted a study to examine the impact of perforations on steel shear walls in comparison to unperforated steel shear walls. For this investigation, three four-story walls were selected. Set (a) comprised unperforated shear walls, while sets (b) and (c) included one circular opening located on the top floor. In addition, for the remaining three floors, set (b) featured 22 openings, whereas set (c) contained 23 openings. All openings were uniformly distributed across the entire surface of the panel, maintaining a horizontal and vertical spacing of 280 mm. Each set consisted of two samples with

distinct beam-to-column connection types: shear and rigid. The findings of this study indicate that, based on the perforation pattern and the relationship between shear strength estimations as outlined in the research conducted by Purba and Bruneau in 2007, the shear strength of the perforated plate is expected to be 0.6 times that of the unperforated plate. Furthermore, the Pushover analysis suggests that this coefficient of 0.6 is a conservative estimate [6].

Roberts and Sabouri-Ghomi [8] performed 16 quasi-static cyclic tests on unstiffened steel shear walls with circular central openings of varying diameters. The panels exhibited stable hysteresis loops and sufficient ductility, while stiffness and ultimate strength decreased linearly with increasing opening diameter. They proposed estimating the reduced strength and stiffness using a factor of $(1 - D/d)$, where $D$ is the hole diameter and $d$ is the panel height.

Deylami and Daftari [9] performed a comprehensive numerical investigation in 2000, analyzing over 50 steel shear wall specimens using the NISA II nonlinear finite element program with pushover analysis. Their research systematically evaluated key geometric parameters - particularly plate thickness, opening aspect ratio, and perforation percentage - to determine the optimal opening configuration.

Pellegrino et al. [10] characterized the linear buckling and post-buckling behavior of perforated steel shear walls under shear loading. Their research analyzed the effects of various factors, including the dimensions and positioning of the opening relative to the two primary axes, the shape of the opening (rectangular and circular), the alignment of the opening with respect to the panel, as well as the wall slenderness and aspect ratio.

Valizadeh et al. [11] experimentally studied the effects of opening and plate slenderness coefficients on the seismic performance of steel shear walls. They tested eight scaled-down specimens (1:6) with two plate thicknesses and four central circular opening ratios under cyclic loading. The openings were placed at the panel center, as this region was found to be the most vulnerable to damage, particularly within the tension zone.

Paslar et al. [12] numerically evaluated steel plate shear walls with different partial connection configurations. Their results showed that systems with mid-height partial connections on vertical boundary elements exhibited advantageous structural behavior. Moreover, when the connection ratio reached 80%, the performance closely matched that of fully connected conventional systems.

Fanaie and Mirsadeghi [13] conducted an experimental study on shear walls with partially connected plates to vertical columns, examining varying discontinuity percentages. Their findings revealed that the discontinuity ratio between the wall and vertical boundary elements significantly impacts the strip model's behavior and the wall's shear capacity. They concluded that discontinuities exceeding 30% are inadmissible.

Jiang et al. [14] have developed and tested a new type of Internally Stiffened Double Steel Plate Shear Wall (ISD-SPSW), demonstrating enhanced load-bearing capacity, ductility, and energy dissipation, while parametric studies showed that reducing wall height and increasing plate thickness improve performance, consistent with finite element simulations.

Wen et al. [15] by experimental and numerical studies on stiffened corrugated steel plate shear walls (S-CSPSWs) showed that adding stiffeners enhances out-of-plane stability and energy dissipation, while early fracture reduces shear capacity. A validated FE model and design formulas for shear resistance were also proposed, matching well with simulation results.

Kordzangeneh et al. [16] by experimental and numerical analyses on SPSWs with square openings showed that increasing opening size notably reduces shear strength (up to 38%) and stiffness (up to 25%), while specimens maintained stable ductile behavior and good energy dissipation until strength degradation occurred around the openings.

A foam-infilled corrugated CFRP–steel sandwich shear wall (CFSSW) was introduced by Feng et al. [17] to enhance load-bearing capacity and energy dissipation of SPSWs. Analytical and FE studies showed that foam infill and CFRP panels improve buckling restraint and hysteretic performance, and simplified design models were proposed for practical application.

Paslar et al. [18] conducted finite element analyses on SPSWs with partially connected infill plates and boundary stiffeners, showing that adding stiffeners increased strength, stiffness, and energy dissipation by up to 16%, 13%, and 14%, respectively, while optimizing plate connections and stiffener geometry improved performance and provided a cost-effective retrofit solution under architectural constraints.

Zhong and colleagues [19] proposed a partially buckling-restrained steel plate shear wall (PBRSPSW) with lightweight bolted restrainers and showed through tests and FE analysis that it achieves up to 95% higher equivalent damping and significantly improved energy dissipation and shear capacity compared to unstiffened ones. They also identified the subplate height-to-thickness ratio as a key design parameter and developed predictive formulas for buckling, stiffness, and hysteretic behavior.

Li et al. [20] investigated the seismic performance of coupled steel plate shear walls with slits (C-SPSWS) through experiments and numerical analyses, showing that the system exhibits stable hysteresis, excellent energy dissipation, and high ductility. Results indicated that optimized coupling beam dimensions and lengths can balance strength, ductility, and material efficiency, with an optimal coupling degree of 0.4–0.6 recommended for seismic design.

Razavi and Bhowmick [21] developed and analyzed self-centering perforated steel plate shear walls (SC-PSPSWs) using OpenSees to assess their seismic performance. Results showed that SC-PSPSWs exhibit smaller residual drifts but about 30% lower peak strength compared to conventional PSPSWs. Although collapse resistance was slightly reduced, the self-centering mechanism effectively minimized post-earthquake residual deformations and economic losses, demonstrating their potential for resilient structural design.

The literature review establishes the foundation for this study's focus on wall-to-boundary-element connections, with particular emphasis on vertical boundary elements. The research specifically investigates how corner truncation configurations and connection length variations affect the wall's lateral load response. In addition to assessing changes in load-bearing capacity, this study will also evaluate several critical performance characteristics including stress distribution patterns, system damping ratios, and cumulative energy dissipation capacity as secondary research objectives.

The novelty of this study lies in (1) proposing and validating a controlled partial discontinuity strategy, (2) identifying the optimal discontinuity ratio that balances boundary demand reduction and tension-field integrity, and (3) providing a practical engineering solution that reflects real construction practices, where plate corners are often cut to avoid stress concentration.

## 2- Development and Verification of Numerical Models

In this study, the ABAQUS [22] finite element software was employed to simulate actual models and conduct numerical analyses. The validity of the modelling approach was first verified by comparing simulation results with experimental data. Upon confirming the accuracy of the model, the modelling approach was utilized to facilitate further analyses. This section details the analytical models, the modelling methodology, and the verification process. To account for the effects of large deformations and to address the non-linear stress-strain behavior of materials, both geometric and material non-linearity were incorporated into the analysis. The implicit Newton-Raphson method was employed due to its compatibility with the elements used in the study. To account for initial imperfections, a linear buckling analysis was first performed on the steel shear wall models. A combination of deformations derived from linear buckling modes, achieved through the application of small coefficients, was utilized as the initial geometric model for the samples in the nonlinear static analysis. The Imperfection command in ABAQUS was employed to introduce these imperfections with an amplitude of 1/1000 of the steel plate height was adopted in all analyses. Following the buckling analysis, a static nonlinear analysis was conducted under cyclic loading to obtain the load-displacement hysteresis curves, incorporating the nonlinear and plastic behavior of the materials. To accurately replicate the experimental setup, two key constraints were implemented: The horizontal boundary element was connected to the vertical boundary element with a hinged connection, while the steel plate was rigidly attached to both the horizontal and vertical boundary elements.

The connection between horizontal and vertical boundary elements was simulated using a hinge constraint. This constraint allows rotation about the axis perpendicular to the steel plate while restraining all other degrees of freedom. For the steel plate connections, a tie constraint was implemented, which fully couples all degrees of freedom between the plate and boundary elements at their connecting nodes. The steel plate was modelled using S4R shell elements, suitable for both thick and thin shell applications. These four-node, doubly curved shell elements employ reduced integration and are capable of modelling three-dimensional shell behavior. The horizontal and vertical boundary elements (HBEs and VBEs) were represented using B31 beam elements. A mesh convergence study determined an optimal element size of 20 mm for both the plate and boundary elements. To simulate material failure, the ductile damage criterion was employed in ABAQUS, incorporating fracture strain (0.227) and stress triaxiality (1/3) to enable element deletion once the specified damage thresholds were reached. Material degradation was defined through the damage evolution sub-option within the ductile damage model, using displacement-based tabular softening and a maximum degradation parameter.

### 2-1- Numerical models

A total of 27 numerical models were developed to analyze the behavior of the investigated steel plate system. The steel plate measures 995 mm × 995 mm, while the overall system -including the neutral web of the horizontal and vertical boundary elements- spans 1195 mm × 1195 mm. The study examines the influence of three key parameters: steel plate thickness (slenderness), the horizontal corner opening percentage (horizontal opening length as a percentage of boundary element length), and the opening aspect ratio (the ratio of horizontal to vertical opening dimensions). A schematic representation of the system is provided in Figure 1.

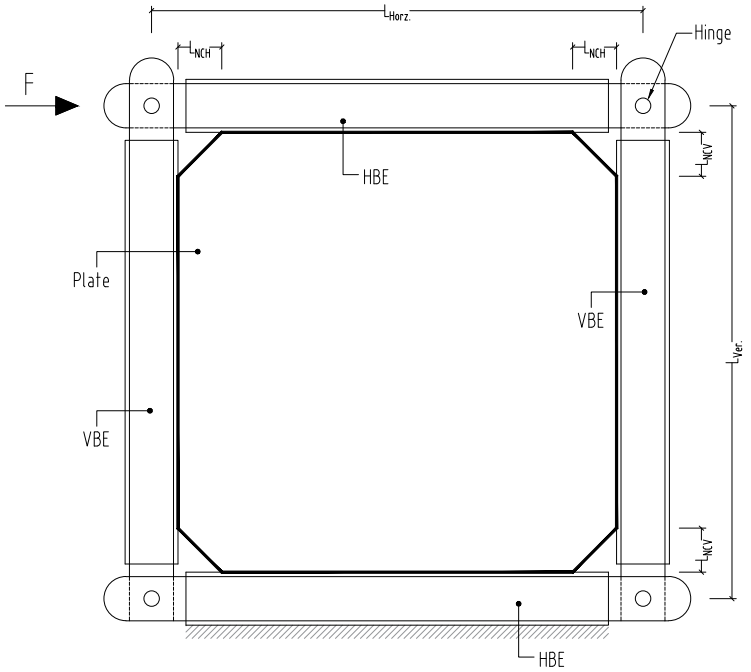


**Figure 1. Schematic View of Studied Model**

**Table 1. Studied parameters and their variation ranges**

| Parameter | Variation interval | Acronym |
|---|---|---|
| Plate thickness (mm) | 1.0, 1.5, 2.0 | t |
| Corner opening horizontal discontinuity percentage (%) | 0, 10, 15, 20, 25 | Dc |
| Opening aspect ratio | 1:1, 1:2, 1:3, 1:4, 1:5 | h/v |

The parameters under investigation, along with their variation ranges, are summarized in Table 1. The plate thickness varies between 1.0, 1.5, and 2.0 mm, while the maximum corner opening percentage ranges from 0% to 25% in increments of 5%. The corner openings percentage refers to the size of openings at the plate's corners expressed as a proportion of the boundary element's total length. For example, a 10% opening means the opening dimension equals 10% of the boundary element length. This parameter helps quantify how much material is removed from the corners, which affects the structural behavior. The study examines opening percentages ranging from 0% to 25% in 5% increments, with special consideration given to treating 0% as equivalent to 5% for analytical purposes. The opening ratio (horizontal:vertical) further defines the shape of these corner openings. The opening ratio, defined as the horizontal-to-vertical discontinuity proportion, includes five configurations: 1:1, 1:2, 1:3, 1:4, and 1:5. As implemented, the 1:3 ratio translated to 5% horizontal and 15% vertical openings.

The detailed configurations of all 27 models are presented in Table 2, specifying plate thickness, vertical and horizontal discontinuity percentages, and their respective ratios. For example, model SW-t1-h5-v5 represents a 1.0 mm thick plate with no openings (5% discontinuity), while SW-t2-h5-v25 corresponds to a 2.0 mm plate with a 5% vertical and 25% horizontal opening, following a 1:5 ratio.

**Table 2. Studied Models**

| Model | Thickness (mm) | Vertical discontinuity (%) | Horizontal discontinuity (%) | Discontinuity ratio |
|---|---|---|---|---|
| SW-t1-h5-v5 | 1 | 5 | 5 | 1:1 |
| SW-t1-h10-v10 | 1 | 10 | 10 | 1:1 |
| SW-t1-h15-v15 | 1 | 15 | 15 | 1:1 |
| SW-t1-h20-v20 | 1 | 20 | 20 | 1:1 |
| SW-t1-h25-v25 | 1 | 25 | 25 | 1:1 |
| SW-t1-h5-v10 | 1 | 5 | 10 | 1:2 |
| SW-t1-h5-v15 | 1 | 5 | 15 | 1:3 |
| SW-t1-h5-v20 | 1 | 5 | 20 | 1:4 |
| SW-t1-h5-v25 | 1 | 5 | 25 | 1:5 |
| SW-t1.5-h5-v5 | 1.5 | 5 | 5 | 1:1 |
| SW-t1.5-h10-v10 | 1.5 | 10 | 10 | 1:1 |
| SW-t1.5-h15-v15 | 1.5 | 15 | 15 | 1:1 |
| SW-t1.5-h20-v20 | 1.5 | 20 | 20 | 1:1 |
| SW-t1.5-h25-v25 | 1.5 | 25 | 25 | 1:1 |
| SW-t1.5-h5-v10 | 1.5 | 5 | 10 | 1:2 |
| SW-t1.5-h5-v15 | 1.5 | 5 | 15 | 1:3 |
| SW-t1.5-h5-v20 | 1.5 | 5 | 20 | 1:4 |
| SW-t1.5-h5-v25 | 1.5 | 5 | 25 | 1:5 |
| SW-t2-h5-v5 | 2 | 5 | 5 | 1:1 |
| SW-t2-h10-v10 | 2 | 10 | 10 | 1:1 |
| SW-t2-h15-v15 | 2 | 15 | 15 | 1:1 |
| SW-t2-h20-v20 | 2 | 20 | 20 | 1:1 |
| SW-t2-h25-v25 | 2 | 25 | 25 | 1:1 |
| SW-t2-h5-v10 | 2 | 5 | 10 | 1:2 |
| SW-t2-h5-v15 | 2 | 5 | 15 | 1:3 |
| SW-t2-h5-v20 | 2 | 5 | 20 | 1:4 |
| SW-t2-h5-v25 | 2 | 5 | 25 | 1:5 |

It is important to note that, among the models examined, an opening percentage of 5 is regarded as nearly unperforated model. This equivalence is established to facilitate the assessment of the hinge node conditions and to evaluate the behavior of the plate in isolation.

The steel material used in the modelling is St37, a commercially available grade and the plastic properties of steel material under cyclic loading were simulated by combining isotropic hardening and kinematic hardening behavior.

## 2-2- Verification

The numerical model was validated by simulating a previously tested specimen, following the assumptions outlined earlier. The study adopts the experimental work of Haji Mirsadeghi and Fanaei [13] due to its relevance to the present research. One of their specimens was modeled in ABAQUS, and the numerical results were compared with experimental data to assess accuracy. For verification, two cases were examined: a model with 30% relative discontinuity (with respect to the vertical boundary element length) and a model with a fully connected steel plate and vertical boundary element.

The specimen dimensions were 300 × 400 mm² with a thickness of 0.3 mm, as shown in Figure 2. The boundary elements consisted of solid square sections (40 × 40 mm²), with the horizontal-to-vertical connection modeled as a hinge. Out-of-plane deformation was restrained, and the lower horizontal boundary element was assumed fixed to replicate experimental conditions.

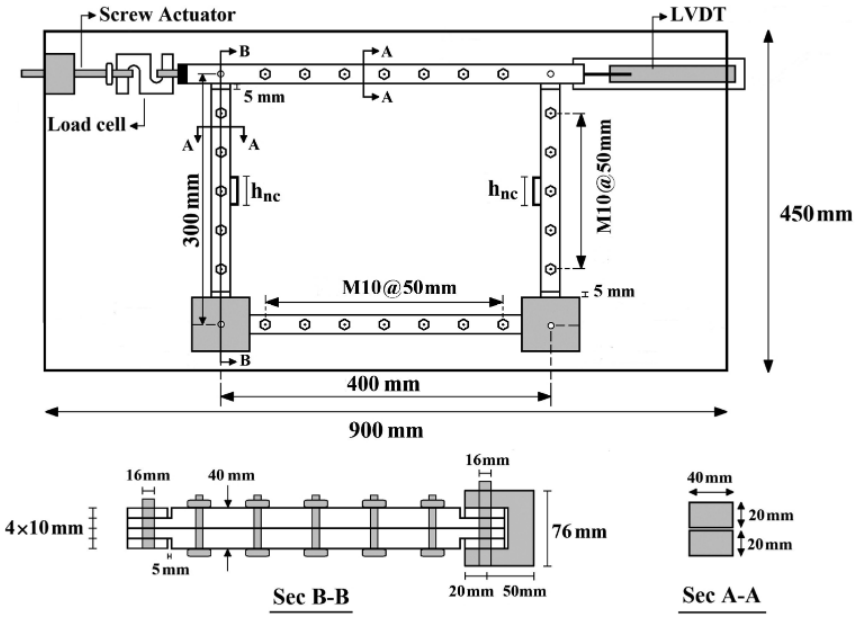


**Figure 2. Dimensions and characteristics of the Mirsadeghi and Fanaei experimental specimen [13]**

First, the fully connected model was analyzed under monotonic loading. The finite element results, presented in Figure 3, demonstrate strong agreement with the experimental data. Next, the model with 30% discontinuity was evaluated, and the numerical predictions again aligned closely with the experimental findings, as illustrated in Figure 4. The consistent validation across both configurations confirms the reliability of the numerical model for investigating steel plate shear wall behavior.

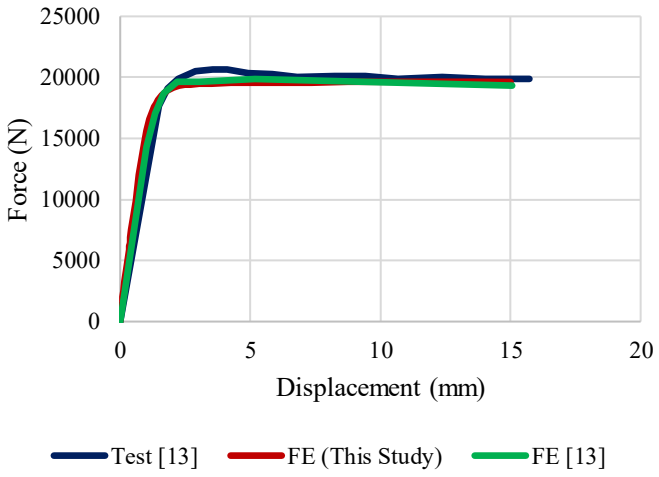


**Figure 3. FE vs. experimental results**

Following the evaluation of the model characterized by a complete connection between the steel plate and the boundary elements, an analysis was conducted on the model exhibiting 30% discontinuity.

Following the completion of the monotonic analyses, the experimental results were compared with those obtained from the finite element analysis, as illustrated in Figure 4. The findings indicate a strong correlation between the numerical analysis and the experimental tests.

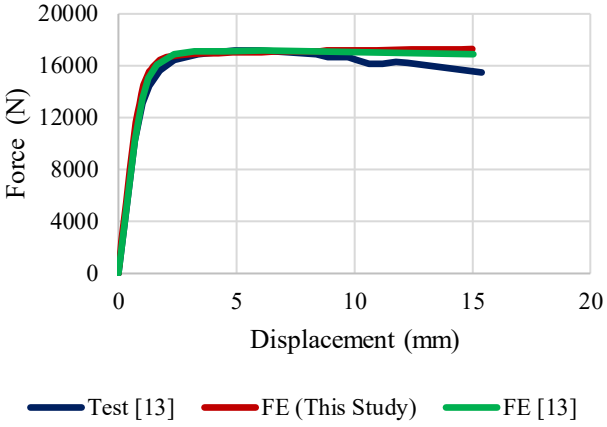


**Figure 4. FE vs. experimental results**

With the numerical model validated, further investigations can now explore the behavior of steel plate shear walls with corner discontinuities.

## 3- Numerical Analysis Results

This section presents the findings from ABAQUS simulations of 27 steel plate shear wall models with varying opening dimensions and aspect ratios. The analysis focuses on five key performance metrics: (1) cyclic and backbone curves, (2) energy dissipation capacity, (3) equivalent viscous damping ratio, (4) effective stiffness, and (5) Deformation behavior. For conciseness, results are presented for 1 mm thick specimens. Additionally, the details of the finite element model are illustrated in Figure 5.

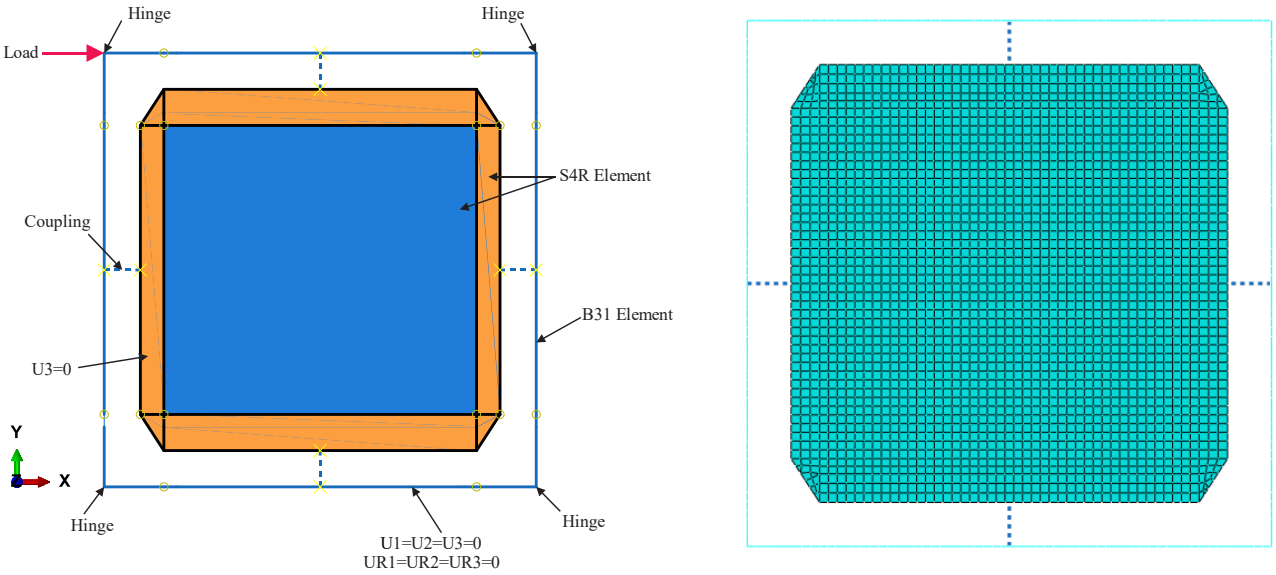


(a) (b)

**Figure 5. (a) Finite Element Model, (b) Meshed Model**

## 3-1- Cyclic and backbone curves

The cyclic curves provide comprehensive insight into the bearing capacity and hysteretic behavior of the steel plate shear walls under cyclic loading. These curves not only reveal the load-carrying capacity but also enable derivation of several key performance indicators, including the backbone (push) curve, energy dissipation characteristics, and equivalent damping ratios. The backbone curve, constructed by connecting the peak points of successive cycles, serves as a particularly important indicator of structural performance, representing the envelope of maximum load resistance.

Figure 6 presents the cyclic response of representative specimens along with their corresponding backbone curves and 85% capacity thresholds. The results demonstrate that specimens with minimal openings exhibit stable hysteretic behavior characterized by gradual stiffness degradation without sudden strength loss. The load-displacement responses show remarkable consistency between positive and negative loading directions across most configurations. However, increasing the opening size produces two notable effects: (1) progressive reduction in load-carrying capacity and (2) more pronounced post-peak strength degradation, as evidenced by steeper descending branches in the backbone curves.

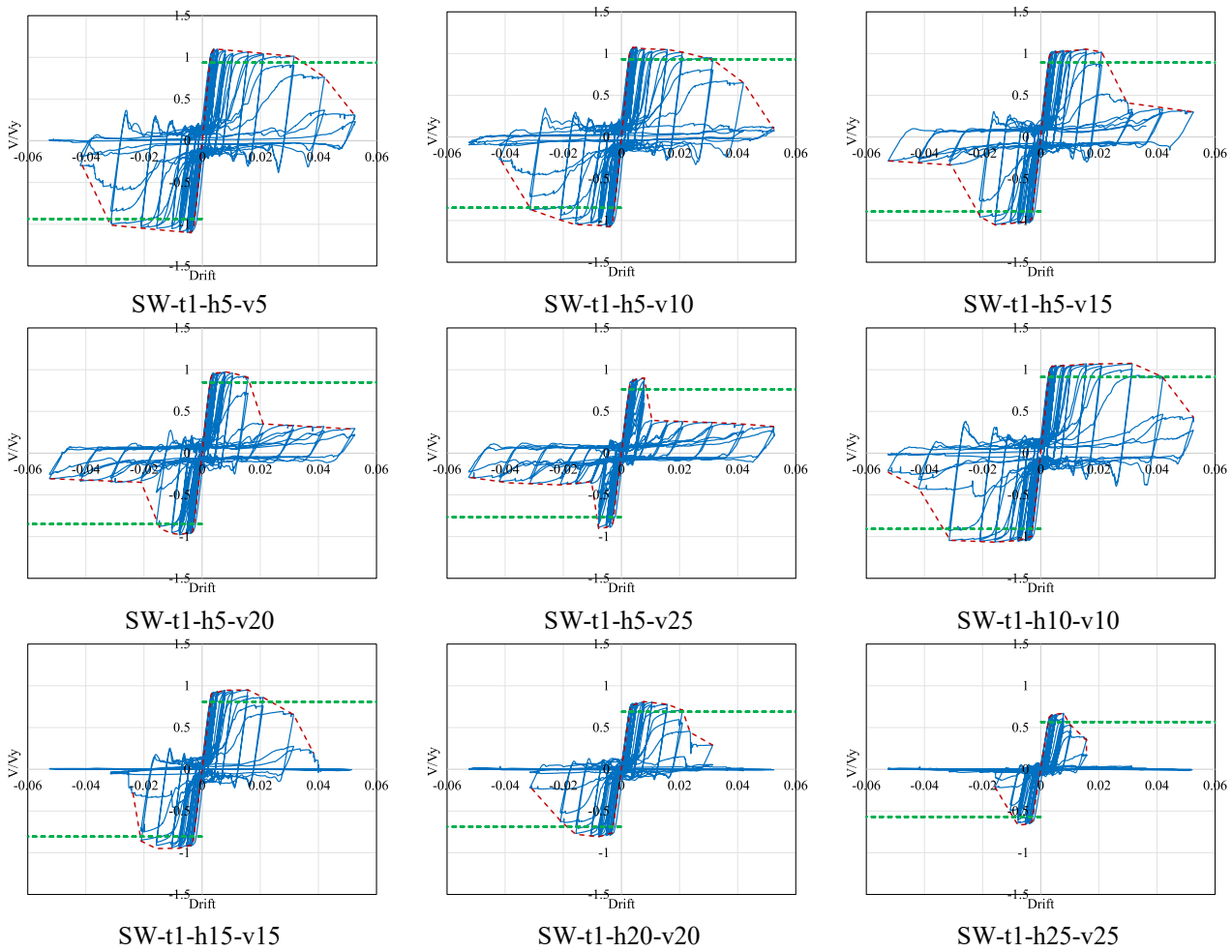


**Figure 6. Cyclic and backbone curves of samples with a thickness of 1 mm.**

According to the Table 3, the mechanical characteristics of each sample can be derived from the Backbone curve. Each parameter listed in the Table 3 is determined in accordance with the guidelines established in FEMA 273 [23].

**Table 3. Mechanical characteristics of samples**

| Specimen | Loading direction | $F_y$ (kN) | $u_y$ (mm) | $F_p$ (kN) | $u_p$ (kN) | $u_u$ (mm) | μ |
|---|---|---|---|---|---|---|---|
| SW-t1-h5-v5 | Positive | 185.59 | 2.87 | 198.09 | 3.93 | 34.83 | 12.15 |
| | Negative | -185.59 | -2.87 | -198.09 | -3.93 | -32.84 | 11.45 |
| SW-t1-h5-v10 | Positive | 179.18 | 2.80 | 193.37 | 3.97 | 30.85 | 11.02 |
| | Negative | -179.18 | -2.80 | -193.37 | -3.97 | -30.85 | 11.02 |
| SW-t1-h5-v15 | Positive | 176.24 | 3.06 | 189.45 | 15.55 | 22.89 | 7.48 |
| | Negative | -176.24 | -3.06 | -189.45 | -15.55 | -22.89 | 7.48 |
| SW-t1-h5-v20 | Positive | 158.77 | 2.84 | 175.12 | 7.81 | 15.92 | 5.60 |
| | Negative | -158.77 | -2.84 | -175.12 | -7.81 | -13.93 | 4.90 |
| SW-t1-h5-v25 | Positive | 151.04 | 2.91 | 161.86 | 7.81 | 9.15 | 3.14 |
| | Negative | -151.04 | -2.91 | -161.86 | -7.81 | -7.86 | 2.70 |
| SW-t1-h10-v10 | Positive | 179.30 | 3.05 | 193.63 | 31.34 | 38.47 | 12.61 |
| | Negative | -179.30 | -3.05 | -191.84 | -15.58 | -33.83 | 11.07 |
| SW-t1-h15-v15 | Positive | 162.28 | 3.17 | 170.89 | 15.68 | 22.89 | 7.21 |
| | Negative | -162.28 | -3.17 | -170.89 | -15.68 | -20.90 | 6.59 |
| SW-t1-h20-v20 | Positive | 136.77 | 3.13 | 145.59 | 7.75 | 20.90 | 6.68 |
| | Negative | -136.77 | -3.13 | -145.59 | -7.75 | -16.92 | 5.41 |
| SW-t1-h25-v25 | Positive | 111.94 | 2.92 | 120.51 | 7.76 | 9.95 | 3.41 |
| | Negative | -111.94 | -2.92 | -120.51 | -7.76 | -9.95 | 3.41 |

The parameters $F_y$ and $u_y$ denote the yield force and the corresponding displacement of the sample, respectively. Similarly, $F_p$ and $u_p$ represent the ultimate force and its associated displacement. Additionally, $F_u$ and $u_u$ correspond to the force and displacement at the point where the sample has achieved 85% of its ultimate capacity. Conversely, an increase in the size of the openings leads to a reduction in the ductility of the model. Notably, the introduction of a 10% opening in the vertical boundary element (as observed in samples h5-v10 and h10-v10) has a considerably lesser effect on diminishing the ductility of the models.

The comprehensive cyclic analysis establishes that while opening size generally reduces capacity and ductility, the effect is nonlinear and configuration-dependent. The subsequent sections will examine how these cyclic characteristics translate to energy dissipation capacity and failure modes under increasing drift demands.

## 3-2- Energy dissipation capacity

The cumulative energy dissipation serves as a key indicator of seismic performance in steel plate shear walls. This parameter is quantified through the area enclosed within each hysteretic loop of the cyclic response curve, representing the energy dissipated during individual loading cycles. Progressive summation of these values at successive drift levels yields the cumulative energy dissipation, which characterizes the system's overall energy absorption capacity throughout the loading history. Figure 7 presents the cumulative energy dissipation behavior for all analyzed configurations.

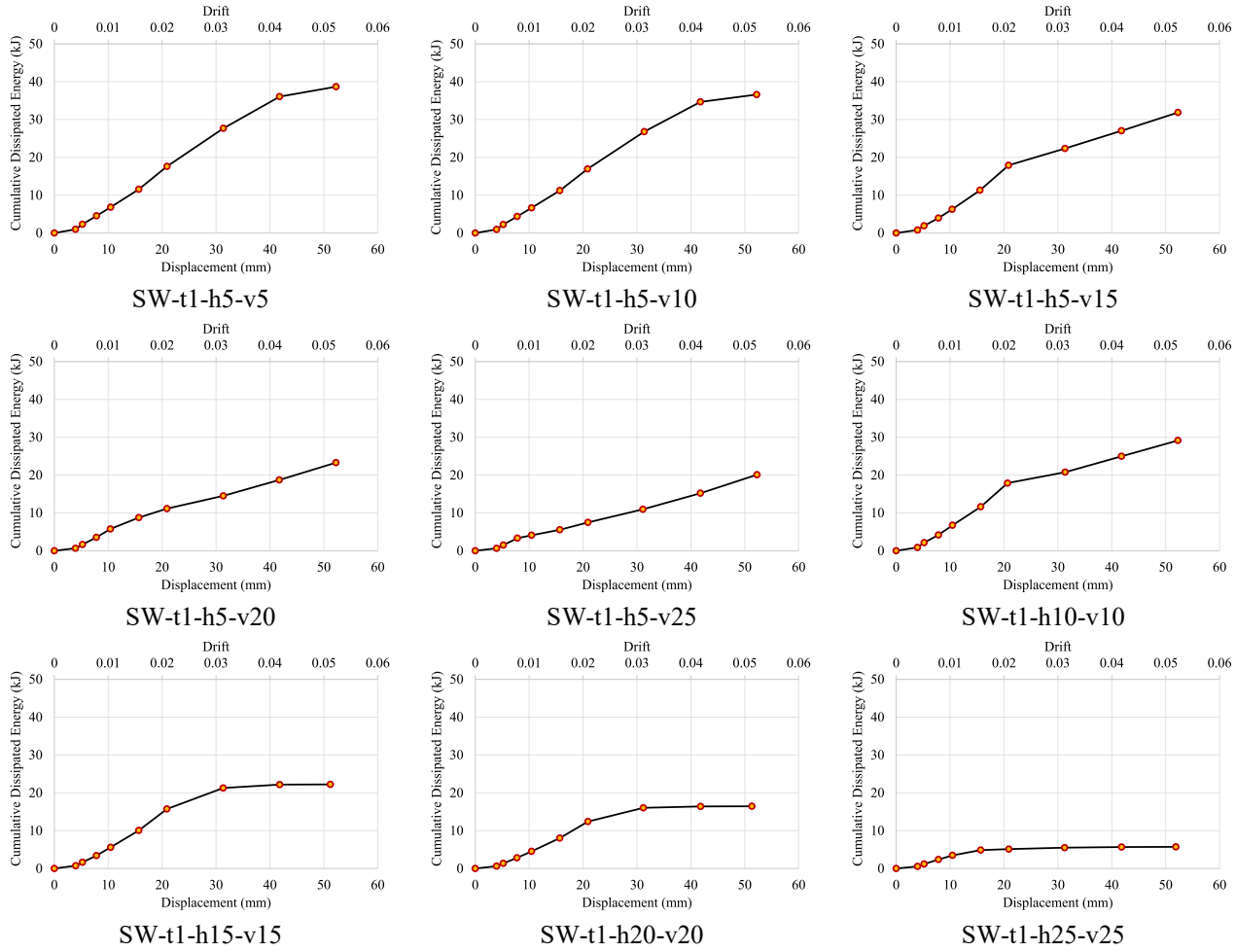


**Figure 7. Cumulative dissipated energy of models with a thickness of 1 mm**

Figure 7 demonstrates distinct energy dissipation patterns among the different models. Specimens with smaller openings maintain a consistent, progressive increase in cumulative energy dissipation throughout the loading history. However, this increasing trend shows notable attenuation in the final cycles as plate damage initiates and progresses. In contrast, models with larger openings - especially those with equal aspect ratios - exhibit significantly reduced energy dissipation capacity, evidenced by near-zero slopes in their cumulative energy curves. This behavior reveals that larger openings substantially diminish the system's ability to dissipate energy through inelastic mechanisms during intermediate loading stages.

The transition in energy dissipation behavior during mid-loading phases correlates directly with plate buckling phenomena and subsequent damage development. Notably, configurations with 10% openings (models h5-v10 and h10-v10) show performance characteristics comparable to solid panels, maintaining stable energy accumulation without sudden reductions in dissipation rate.

The comprehensive results confirm that opening configuration significantly influences energy dissipation performance. Unequal aspect ratio openings consistently outperform equal ratio configurations, exhibiting more reliable hysteretic behavior and maintaining superior energy absorption capacity throughout the loading protocol.

## 3-3- Equivalent viscous damping ratio

The equivalent viscous damping ratio serves as a fundamental metric for evaluating the energy dissipation characteristics of the structural systems and calculated as shown in Figure 8. This parameter is calculated as the ratio of the hysteretic energy dissipated per cycle (represented by the area enclosed within each load-displacement loop) to the elastic strain energy of an equivalent linear system. Figure 9 presents the evolution of this damping ratio across various drift levels for all specimen configurations.

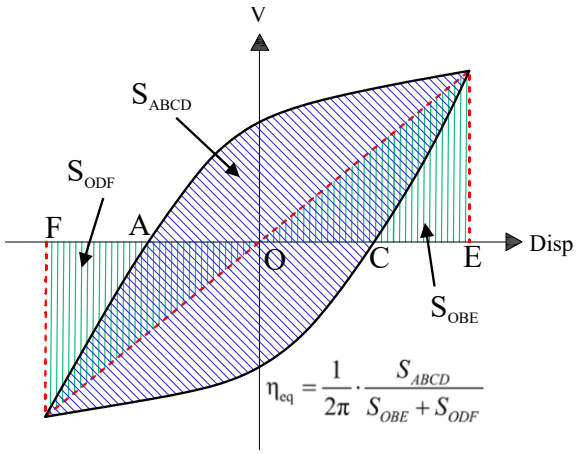


**Figure 8. Calculation diagram of equivalent viscous damping ratio**

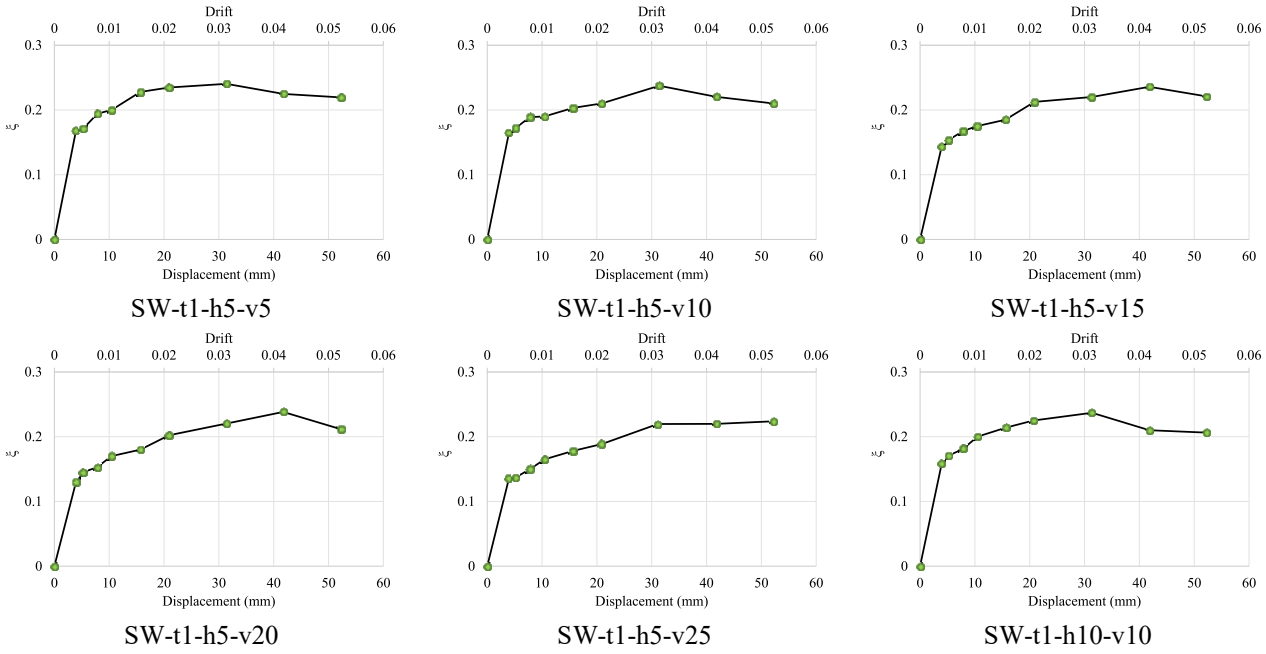

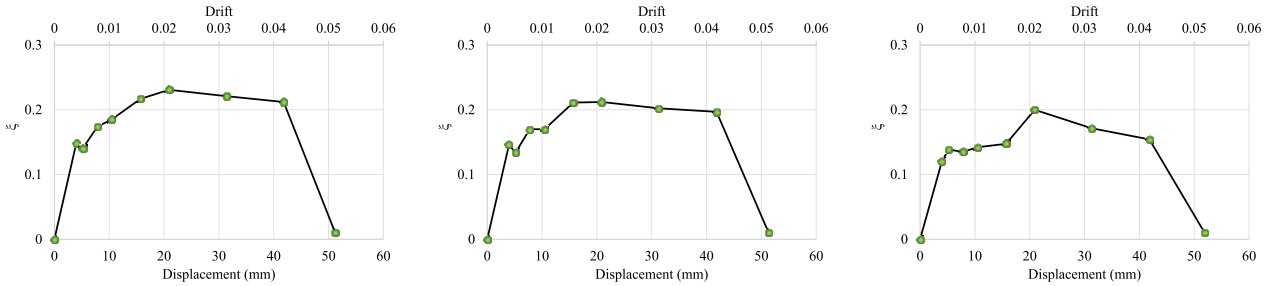


**Figure 9. Equivalent viscous damping ratio for 1 mm thick specimens with varying opening configurations.**

The results reveal three distinct behavioral phases in the damping ratio development. Initially, most specimens show a progressive increase in damping capacity until plate buckling occurs, which interrupts this trend. Following buckling, the damping ratio resumes its upward trajectory but at a reduced rate. The final phase commences when significant plate damage accumulates, causing the damping ratio to decline despite continued energy dissipation.

For specimens with larger openings, the damping ratio curve develops a negative slope beginning at mid-range drift levels, showing a significantly steeper rate of decline. In contrast, specimens with smaller opening ratios exhibit a more gradual descending slope in their damping ratio curves.

The results clearly demonstrate that models with unequal opening configurations outperform those with equal openings. This superior performance is particularly evident in the damping ratio behavior, where equal-opening models show an abrupt reduction in equivalent viscous damping that initiates at intermediate drift levels.

## 3-4- Effective stiffness

The effective stiffness ($K_{eff}$) serves as a key indicator of the system's resistance to lateral deformations. Calculated according to FEMA 273 guidelines (Eq. 1), this parameter quantifies the secant stiffness at each drift level by averaging the absolute peak forces and displacements from positive and negative loading cycles:

$$K_{eff} = \frac{|F_{max}^{+}| + |F_{max}^{-}|}{|u_{max}^{+}| + |u_{max}^{-}|} \quad (1)$$

In this context, $F_{max}^{+}$ and $F_{max}^{-}$ represent the maximum positive and negative force values tolerated during each cycle, while $u_{max}^{+}$ and $u_{max}^{-}$ denote the displacements associated with these forces. Figure 10 illustrates the effective stiffness of the models in relation to the corresponding drifts.

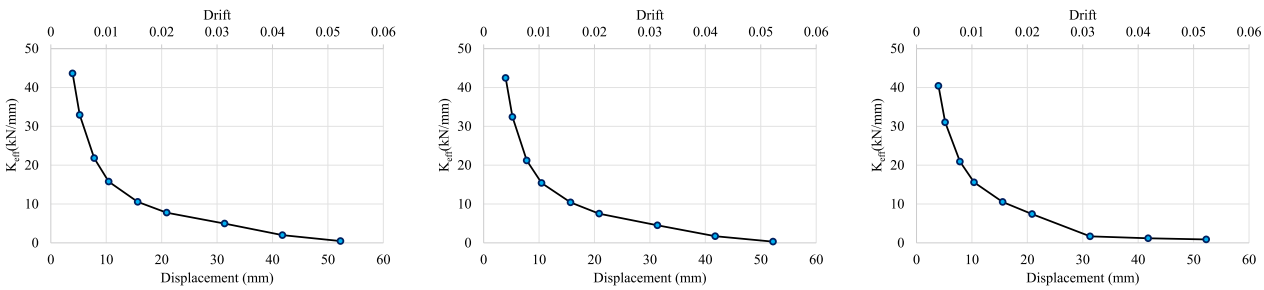

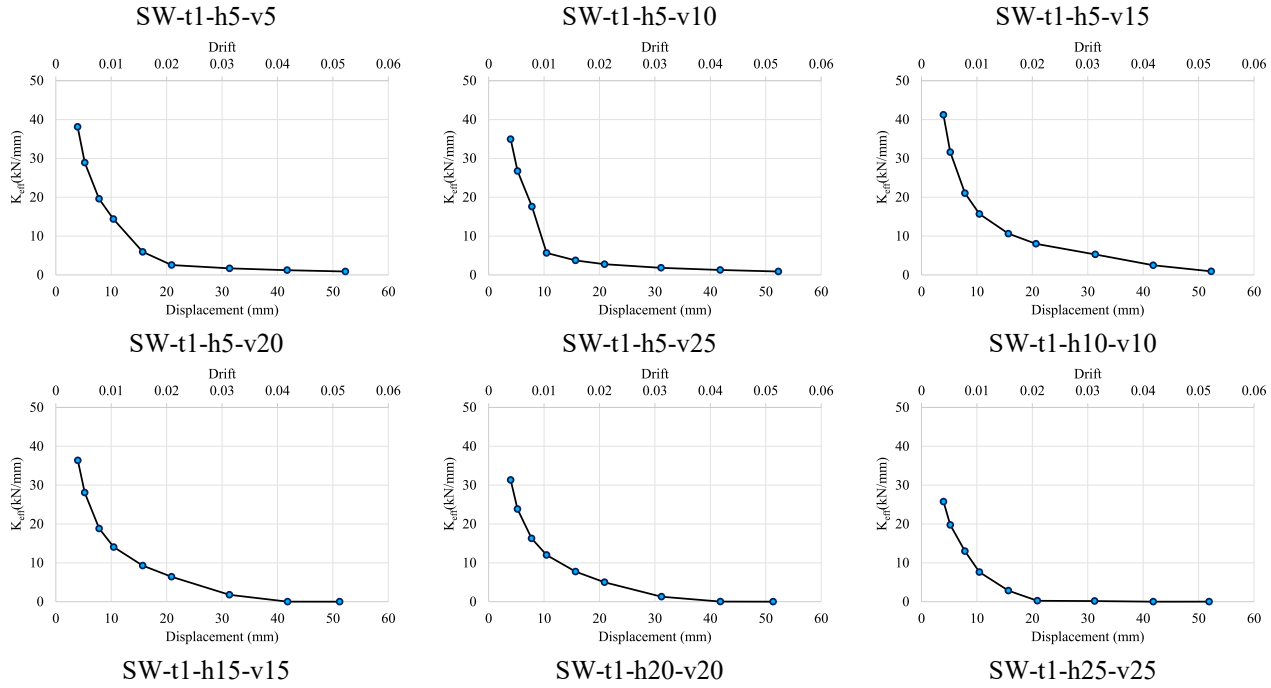


**Figure 10. Effective stiffness for 1 mm thick specimens with varying opening configurations.**

The observed plate damage and associated deformations at higher drift levels directly reduce the system's capacity to resist lateral deformations, consequently decreasing the effective stiffness. This trend aligns with previous parametric analyses, where models with unequal opening dimensions consistently outperformed those with equal dimensions. Notably, specimens featuring 10% openings (h5-v10 and h10-v10) demonstrated superior behavior compared to other configurations.

## 3-5- Deformation behavior

The deformation characteristics at 2% and 4% drift levels, shown in Figure 11, provide critical insight into the system's failure mechanisms. Examination of these deformed configurations enables detailed evaluation of tension field development, stress concentrations near boundary elements, and damage progression patterns under various opening conditions.

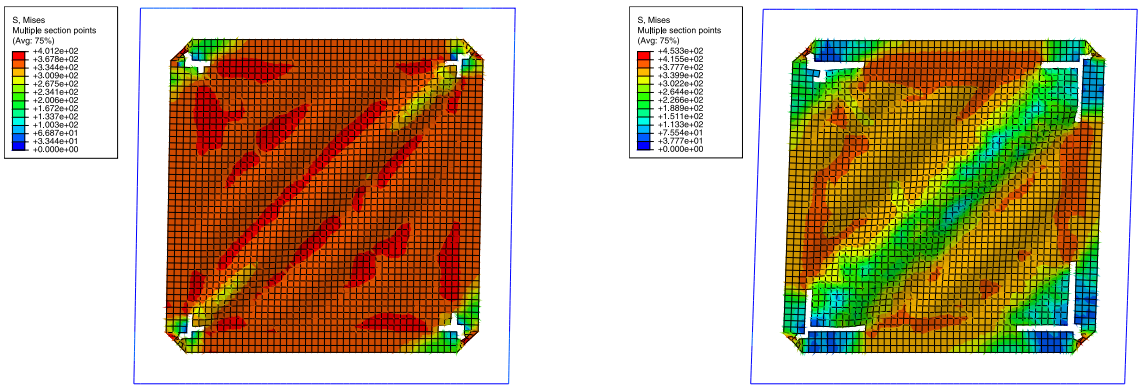


a. SW-t1-h5-v5 – Drift 2%

b. SW-t1-h5-v5 – Drift 4%

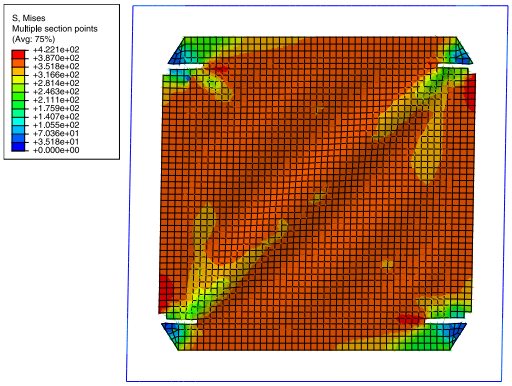


c. SW-t1-h5-v10 – Drift 2%

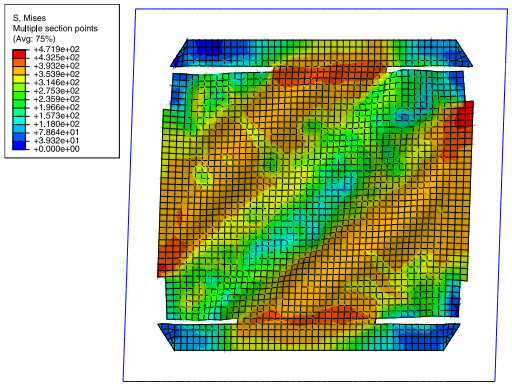


d. SW-t1-h5-v10 – Drift 4%

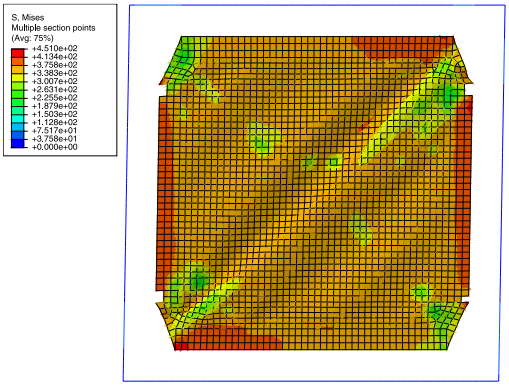


e. SW-t1-h5-v15 – Drift 2%

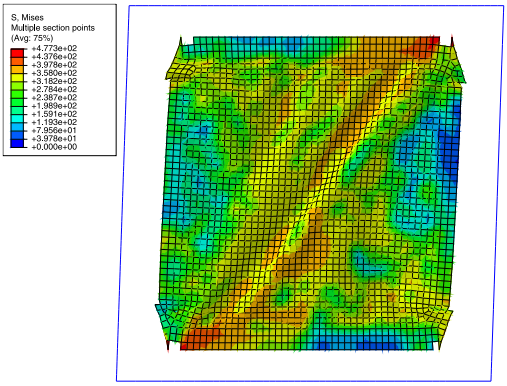


f. SW-t1-h5-v15 – Drift 4%

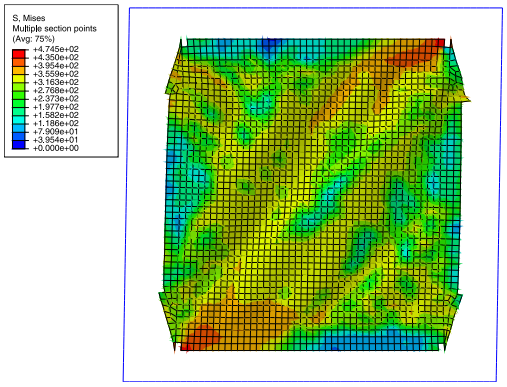


g. SW-t1-h5-v20 – Drift 2%

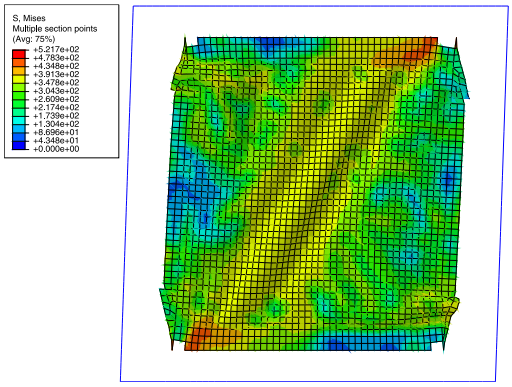


h. SW-t1-h5-v20 – Drift 4%

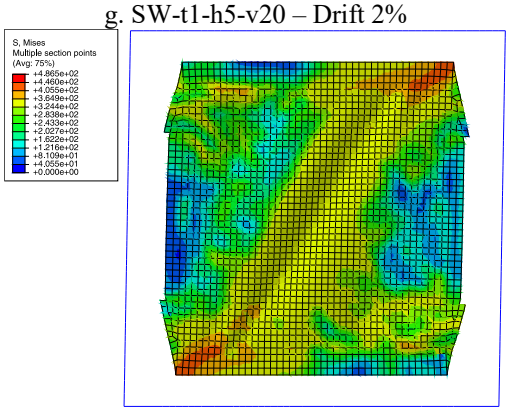


i. SW-t1-h5-v25 – Drift 2%

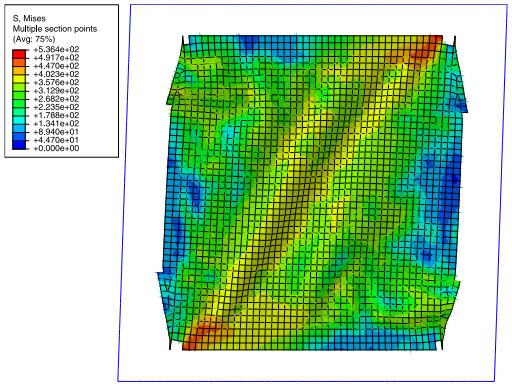


j. SW-t1-h5-v25 – Drift 4%

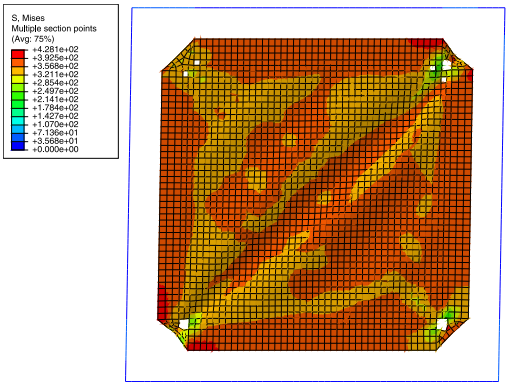


k. SW-t1-h10-v10 – Drift 2%

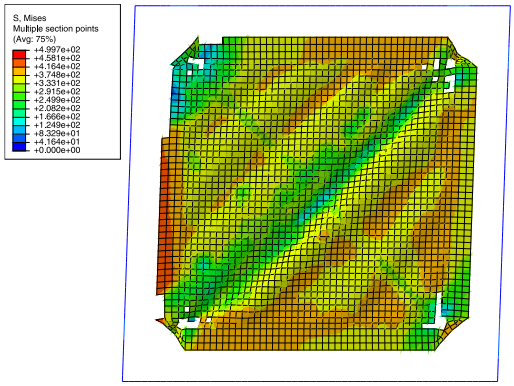


l. SW-t1-h10-v10 – Drift 4%

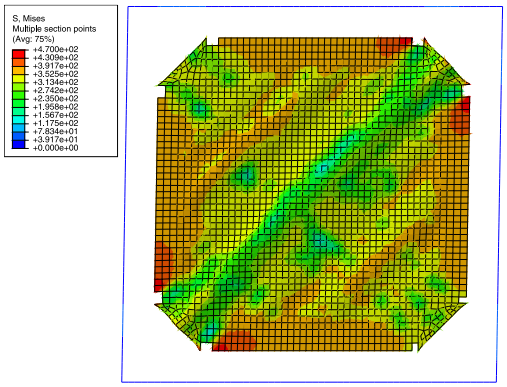


m. SW-t1-h15-v15 – Drift 2%

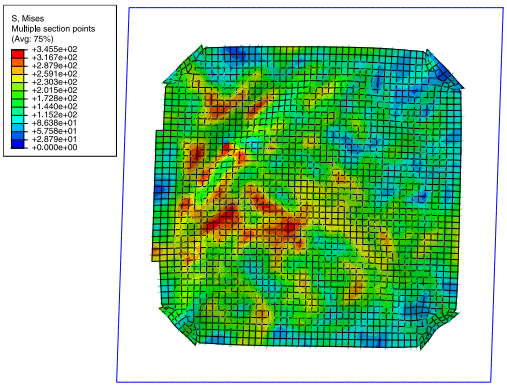


n. SW-t1-h15-v15 – Drift 4%

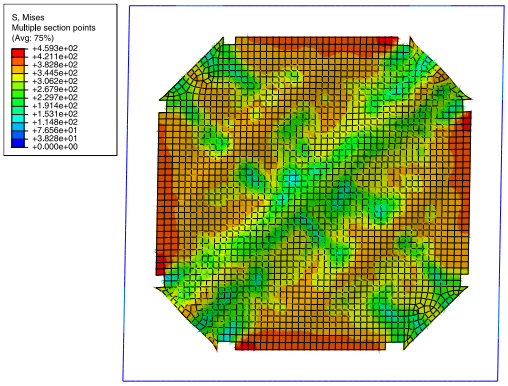


o. SW-t1-h20-v20 – Drift 2%

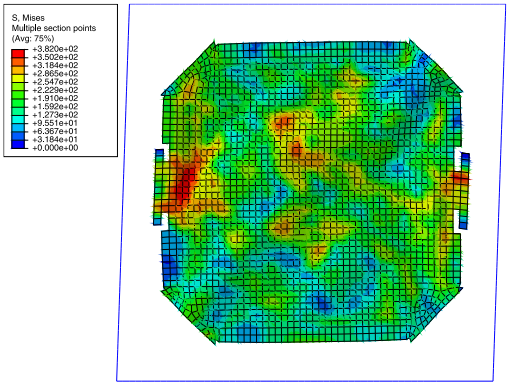


p. SW-t1-h20-v20 – Drift 4%

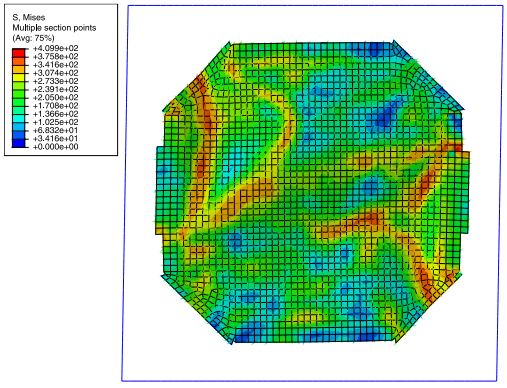


q. SW-t1-h25-v25 – Drift 2%

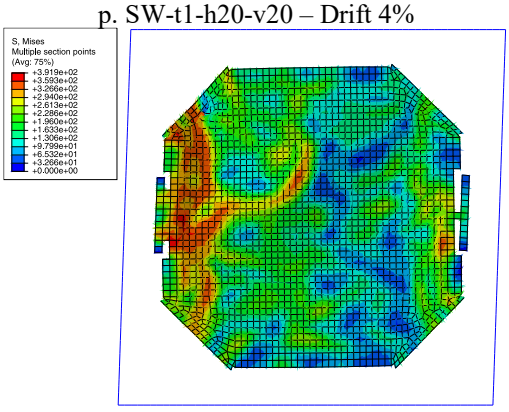


r. SW-t1-h25-v25 – Drift 4%

**Figure 11. The deformed shapes in drifts of 2% and 4% for 1 mm thick specimens with varying opening configurations.**

Analysis of Figure 11 demonstrates that increased opening percentages significantly disrupt tension field development, leading to accelerated plate failure. Across all models, failure initiates consistently at plate corners before propagating either inward toward the center (in specimens with smaller openings) or outward along boundary elements (in models with larger openings). Specifically, specimens with 20-25% openings show damage initiating directly at horizontal and vertical boundary elements, followed by progressive failure propagation along these critical members.

This failure pattern near boundary elements severely compromises load paths, resulting in substantial reductions of both structural strength (5-40% decrease) and system ductility (5-75% reduction) compared to solid panel benchmarks. Models with larger openings exhibit additional behavioral complexities, developing pronounced out-of-plane deformations at relatively low drift levels (1.25-2.0%), as clearly reflected in their load-displacement responses. Although the demand on the boundary elements is diminished in models with large openings, the reduced connected length between the plate and the boundary element renders them incapable of withstanding the demands imposed by the plate. Consequently, at higher drift levels, these elements experience failure, leading to a marked decrease in their load-carrying capacity.

In contrast, unperforated models and those with 10-15% openings maintain stable deformation characteristics throughout loading. Among all investigated configurations, unequal opening arrangements demonstrate superior performance, showing more favorable damage progression patterns and delayed failure initiation.

Following individual examination of the models, subsequent sections will provide comparative analysis of their behaviors. To facilitate more efficient and straightforward comparison, the models will be categorized and analyzed separately based on whether they have equal or unequal openings.

## 3-6- Comparative Analysis of Equal-Opening Models

### 3-6-1- Backbone curve characteristics

Figure 12 compares and examines the backbone curves of models with identical opening sides. The data presented in this figure indicate that in models with equal opening dimensions, increasing the opening size significantly reduces both strength and ductility while moderately decreasing stiffness. The deformation capacity is also adversely affected, with the 25% opening model failure before reaching 2% drift. In contrast, models without openings and those with 10% openings show favorable performance in strength, stiffness, and ductility. While increased plate thickness does not substantially affect the backbone curve, the hysteresis curves discussed previously demonstrate that greater thickness can delay plate failure in some cases.

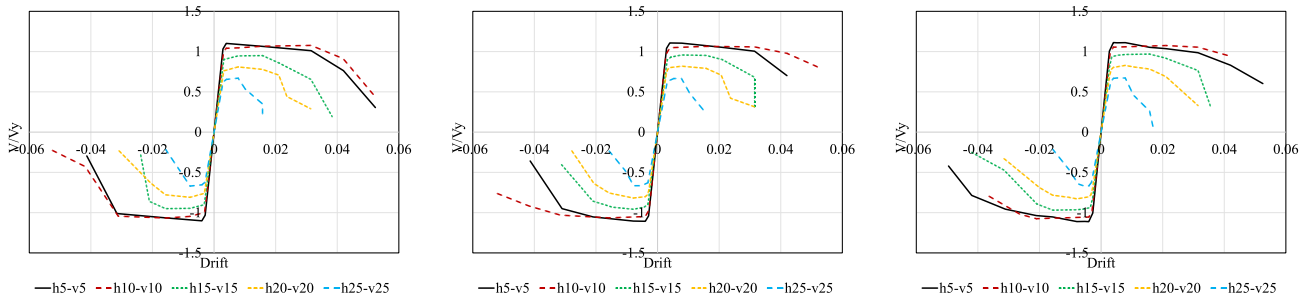


a. SW-t1 b. SW-t1.5 c. SW-t2

**Figure 12. Comparative Analysis of Backbone Curves of Models with Identical Openings Sides.**

## 3-6-2- Energy dissipation capacity

Following analysis of the backbone curve in Figure 13, the cumulative dissipated energy curves for models with equal opening sides are compared. As previously discussed, the cumulative dissipated energy at each drift level equals the total area under the force-displacement curve up to that drift point.

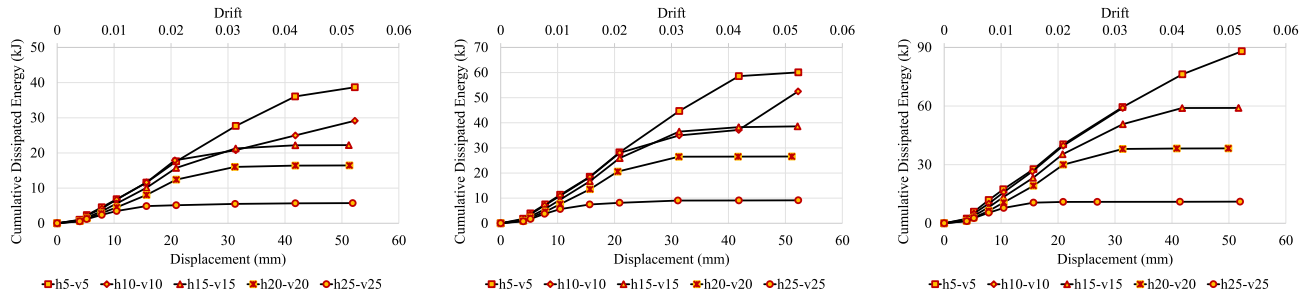


a. SW-t1 b. SW-t1.5 c. SW-t2

**Figure 13. Comparative Analysis of Cumulative Dissipated Energy Curves for Models with Identical Opening Dimensions**

The analysis in Figure 13 shows that comparing cumulative dissipated energy curves for models with identical opening dimensions reveals a positive thickness-energy dissipation correlation. Specifically, as thickness increases, the 10% opening model's energy dissipation characteristics become increasingly similar to those of the unperforated model. Both unperforated models and 10% opening models demonstrate stable energy dissipation during loading.

In contrast, other models show significant reduction in cumulative energy dissipation curve slope during initial loading drifts. This results from plate buckling and substantial out-of-plane deformation causing damage. Consequently, energy dissipation for 20% and 25% opening models effectively reaches zero midway through loading. However, the 15% opening model performs better at 2 mm thickness than at 1 mm or 1.5 mm thicknesses.

## 3-6-3- Effective stiffness degradation

Figure 14 presents a comparative analysis of the effective stiffness curves for models with identical opening percentages. As discussed in previous sections, effective stiffness refers to the model’s capacity to resist horizontal deformations.

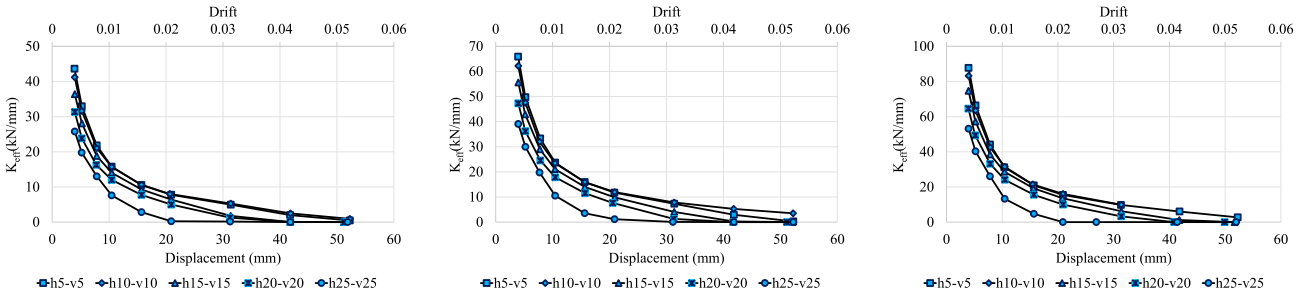


a. SW-t1 b. SW-t1.5 c. SW-t2

**Figure 14. Comparative Analysis of Effective Stiffness Curves for Models with Identical Opening Percentages**

The data in Figure 14 indicate that as the opening percentage increases, the effective stiffness at the onset of loading decreases. Notably, the rate of stiffness reduction remains consistent across all models (except those with a 25% opening) up to a 3% drift. However, during the final loading cycles, models with larger openings experience accelerated failure, causing their effective stiffness to approach zero more rapidly than in other models.

Consistent with earlier observations, models without openings and those with a 10% opening exhibit more stable behavior. Additionally, an analysis of model slenderness reveals that in samples with reduced slenderness (2 mm thickness), the stiffness degradation rate varies. Specifically, samples with openings smaller than 20% demonstrate delayed failure compared to those with larger openings.

## 3-6-4- Equivalent viscous damping behavior

Figure 15 compares the equivalent viscous damping ratio curves for models with identical opening percentages. The curves in Figure 13 reveal that slenderness has a negligible influence on the equivalent viscous damping ratio. The highest damping ratio (~25%) occurs in the model without openings. Consistent with prior observations, models without openings—along with those featuring 10% and 15% openings—display more stable behavior than other configurations. In contrast, samples with 20% and 25% openings exhibit a sharp decline in the equivalent viscous damping ratio, likely due to premature failure and significant out-of-plane deformations.

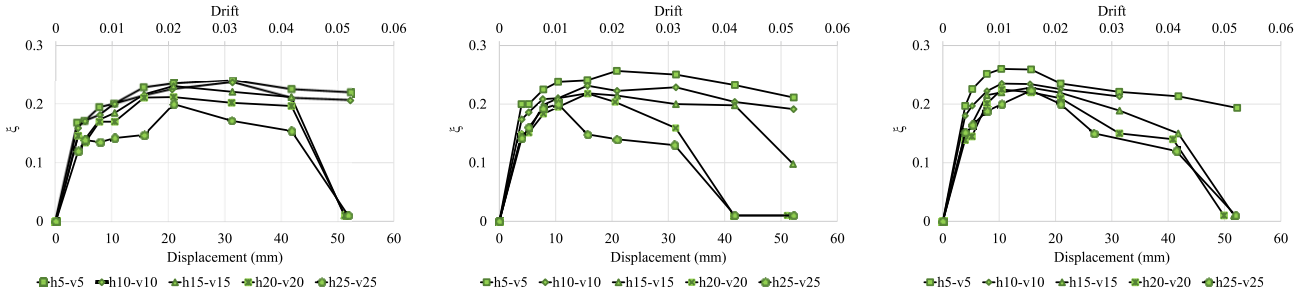


a. SW-t1 b. SW-t1.5 c. SW-t2

**Figure 15. Comparison of equivalent viscous damping ratio curves for samples with equal opening percentages.**

## 3-7- Comparative Analysis of Unequal-Opening Models

### 3-7-1- Backbone curve characteristics

Figure 16 presents a detailed comparison of the backbone curves for models with unequal opening percentages. As shown in this Figure, models with unequal openings exhibit a significant reduction in strength, ductility, and stiffness as the opening size on the vertical boundary element increases. Another critical observation is the reduced deformation capacity of the models. Notably, the specimen with a 25% opening failed before reaching 2% drift, demonstrating significantly lower ductility compared to other configurations.

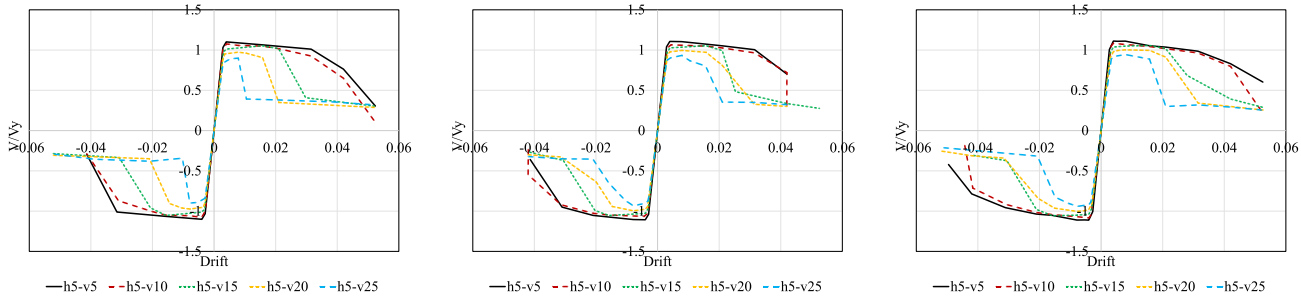


a. SW-t1 b. SW-t1.5 c. SW-t2

**Figure 16. Comparison of backbone curves for models with unequal opening percentages.**

Consistent with previous findings, models without openings and those with a 10% opening demonstrate superior performance in strength, stiffness, and ductility. While increasing plate thickness has a negligible effect on the backbone curve and ductility, hysteresis curves (discussed earlier) indicate that greater thickness can delay plate failure in some cases.

A key observation is that models with unequal openings has significantly better performance than those with equal openings. For example, the model with a 25% unequal opening retained residual capacity even after failure initiation, sustaining minimal load-bearing capability throughout the loading process.

### 3-7-2- Energy dissipation capacity

Following the analysis of the backbone curve, the cumulative dissipated energy curves for models with unequal opening percentages are compared in Figure 17. As previously discussed, the cumulative dissipated energy at each drift level is defined as the total area under the force-displacement curve up to the respective drift point.

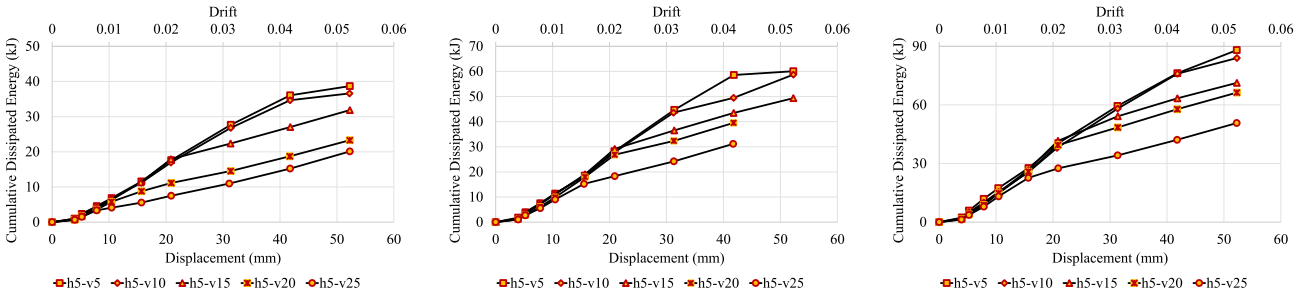


a. SW-t1 b. SW-t1.5 c. SW-t2

**Figure 17. Comparison of Cumulative Dissipated Energy Curves for Models with Unequal Opening Percentages.**

Figure 17 shows that a reduction in slenderness (i.e., an increase in thickness) correlates with improved energy dissipation capacity. Additionally, as thickness increases, the energy dissipation capacity of the model with 10% opening approaches that of the solid model (no openings). The figure also reveals that both the model without openings and the 10% opening model exhibit stable energy absorption behavior during loading. In contrast, the other models show a gradual decline in the slope of their cumulative energy dissipation curves during initial loading drifts, attributed to buckling and significant out-of-plane plate deformations, which ultimately lead to damage.

Unlike models with equal opening percentages, no zero slope is observed in the cumulative dissipated energy curves for these cases, indicating that energy dissipation capacity remains non-zero throughout all loading cycles. Furthermore, the model with a 20% opening performs better at a thickness of 2 mm (lower slenderness) compared to thicknesses of 1 mm and 1.5 mm (higher slenderness).

## 3-7-3- Effective stiffness degradation

Figure 18 presents a comparative analysis of the effective stiffness curves for models with unequal opening percentages. As discussed in previous sections, effective stiffness represents a sample's capacity to resist horizontal deformations.

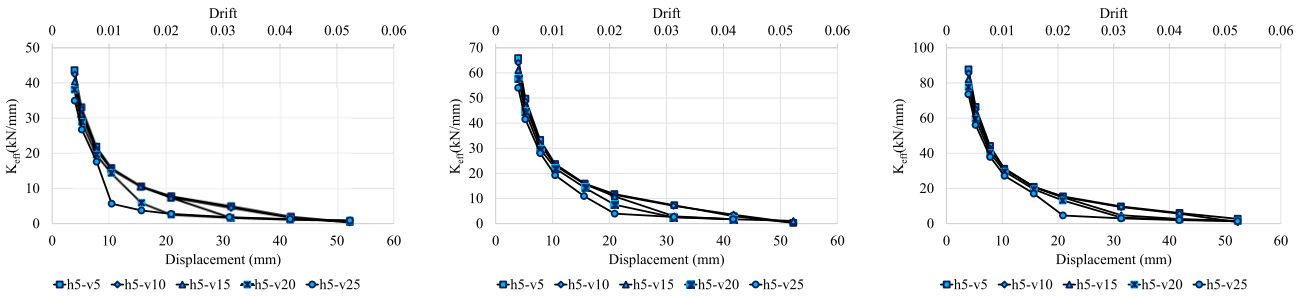


a. SW-t1 b. SW-t1.5 c. SW-t2

**Figure 18. Comparison of effective stiffness degradation for models with unequal opening percentages**

As illustrated in Figure 18, models with unequal openings exhibit distinct behavior compared to those with equal openings. Specifically, the initial effective stiffness at the onset of loading remains relatively consistent across models, regardless of the opening percentage. Notably, the rate of stiffness degradation is similar in all models—except for the 25% opening case—up to a 3% drift. However,

during the final loading cycles, models with larger openings experience failure more rapidly, causing their effective stiffness to approach zero.

Consistent with prior observations, both the solid model (no openings) and the 10% opening model demonstrate more stable behavior than the others in the final cycles, maintaining their load-bearing capacity without a sharp or sudden drop in stiffness. Furthermore, an analysis of plate slenderness shows that in models with lower slenderness (2 mm thickness), the stiffness degradation rate varies. Specifically, samples with openings below 20% exhibit delayed failure compared to those with higher opening percentages.

### 3-7-4- Equivalent viscous damping behavior

Figure 19 compares the equivalent viscous damping ratio curves for models with unequal opening percentages. The curves in Figure 19 reveal that slenderness has a negligible influence on the equivalent viscous damping ratio, with the maximum value (approximately 25%) occurring in the solid model (no openings). Additionally, the viscous damping ratio remains unaffected by whether the opening percentages are equal or unequal.

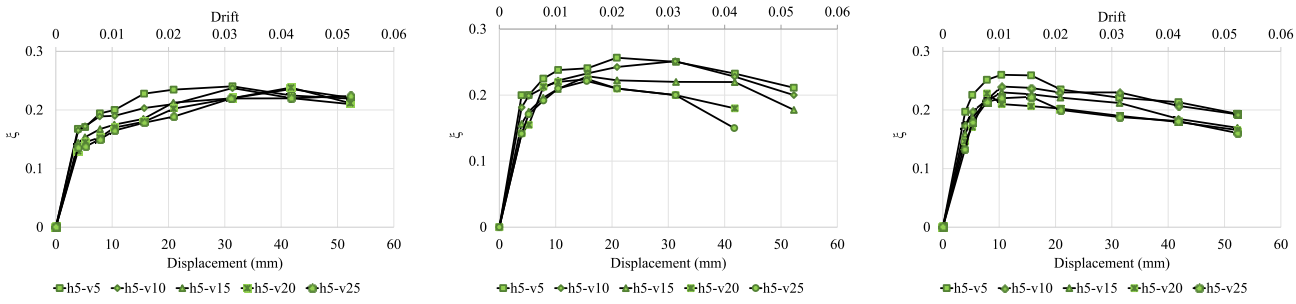


a. SW-t1 b. SW-t1.5 c. SW-t2

**Figure 19. Comparison of equivalent viscous damping ratio for models with unequal opening percentages.**

Consistent with prior observations—and unlike samples with equal openings—models featuring unequal openings exhibit more stable behavior throughout loading. In these cases, buckling, significant out-of-plane deformations, and plate damage only occur during the final loading cycles. As a result, the viscous damping ratio decreases gradually rather than abruptly.

## 4- Conclusion

Steel plate shear walls (SPSWs) typically impose heavy demands on horizontal and vertical boundary elements, necessitating conservative design approaches. This study proposed a methodology to mitigate these demands, particularly for vertical boundary elements, which do not benefit from force cancellation effects observed in multi-story horizontal elements. A comprehensive analysis of 27 SPSW models-with thicknesses of 1 mm, 1.5 mm, and 2 mm and varying percentages of equal/unequal horizontal/vertical openings-was conducted. Key outcomes, including cyclic response, backbone curves, energy dissipation, stiffness degradation, damping ratios, and failure modes, were evaluated. The findings are summarized as follows.

The results highlight several key behavioral aspects of the studied steel plate shear wall models. Increasing the opening ratio beyond 10% leads to premature plate buckling and out-of-plane deformations, resulting in reduced strength and deformation capacity. One of the primary reasons why increasing the size of corner openings reduces the strength and induces large deformations is the disruption of the tension-field action. This disruption predominantly affects the boundary columns rather than the beams, because the influence of the tension field on beams in consecutive stories tends to neutralize each other, whereas columns directly carry the concentrated forces induced by the tension field. Nevertheless, models with unequal openings of ≤10% demonstrate near-optimal cyclic and backbone curve responses, showing close agreement with the performance of solid-plate configurations. Variations in plate thickness -and consequently in slenderness- exerted negligible influence on the overall failure behavior of the system. All models exhibited consistent failure patterns, indicating that slenderness is not a dominant design parameter for the examined configurations. In terms of energy dissipation, cumulative energy absorption decreased as the opening length increased. While models with equal openings exhibited minor variations in dissipated energy across cycles at higher loading levels, those with unequal openings maintained positive energy dissipation slopes, reflecting stable hysteretic behavior. Particularly, models with unequal openings ≤10% showed superior energy dissipation stability. Regarding stiffness degradation, equal-opening models experienced a noticeable reduction in initial stiffness with increasing opening size, whereas unequal-opening models preserved comparable initial stiffness. However, both configurations displayed accelerated stiffness degradation due to disruption of the tension field and localized boundary damage. Models incorporating ≤10% unequal openings retained appreciable stiffness up to the final loading cycles. Finally, in terms of damping behavior, equal-opening models exhibited abrupt stiffness loss and a significant reduction in equivalent viscous damping -approaching near-zero levels- during intermediate cycles. Conversely, unequal-opening models demonstrated gradual degradation, with buckling and damage delayed until the final cycles, thereby maintaining greater damping stability throughout loading.

Introducing openings increases out-of-plane deformations and reduces the wall's performance, while simultaneously decreasing the demand on the boundary elements. However, it should be noted that the precise size of the openings has never been explicitly addressed. Current study demonstrates that steel plate shear walls with unequal openings ≤10% achieve stable, code-compliant behavior while significantly reducing demands on vertical boundary elements. Their cyclic performance, energy dissipation, and stiffness characteristics closely resemble those of solid-plate systems, validating their viability as a design alternative. Future research should focus on optimizing opening geometries (e.g., shape, distribution) and investigating their effects in multi-panel systems to further enhance efficiency and applicability.

## 5- References


1. Berman, J. W., & Bruneau, M. (2005). Experimental investigation of light-gauge steel plate shear walls. Journal of Structural Engineering, 131(2), 259-267.
2. Vian, D., & Bruneau, M. (2004). Testing of special LYS steel plate shear walls. 13th World Conference on Earthquake Engineering, Vancouver, British Columbia, Canada.
3. Vian, D. (2005). Steel plate shear walls for seismic design and retrofit of building structures [Doctoral dissertation, State University of New York at Buffalo].
4. Vian, D., Bruneau, M., Tsai, K.-C., & Lin, Y.-C. (2009). Special perforated steel plate shear walls with reduced beam section anchor beams. I: Experimental investigation. Journal of Structural Engineering, 135(3), 211-220.

5. Vian, D., Bruneau, M., & Purba, R. (2009). Special perforated steel plate shear walls with reduced beam section anchor beams. II: Analysis and design recommendations. Journal of Structural Engineering, 135(3), 221-228.
6. Purba, R., & Bruneau, M. (2007). Design recommendations for perforated steel plate shear walls (MCEER Report No. 07-0011). Multidisciplinary Center for Earthquake Engineering Research.
7. Moghimi, H., & Driver, R. G. (2011). Effect of regular perforation patterns on steel plate shear wall column demands. In Structures Congress 2011 (pp. 2101-2112). ASCE.
8. Roberts, T. M., & Sabouri-Ghomi, S. (1992). Hysteretic characteristics of unstiffened perforated steel plate shear panels. Thin-Walled Structures, 14(2), 139-151.
9. Deylami, A., & Daftari, H. (2000). Non-linear behavior of steel plate shear wall with large rectangular opening. 12th World Conference on Earthquake Engineering, Auckland, New Zealand.
10. Pellegrino, C., Maiorana, E., & Modena, C. (2009). Linear and non-linear behaviour of steel plates with circular and rectangular holes under shear loading. Thin-Walled Structures, 47(6-7), 607-616.
11. Valizadeh, H., Sheidaii, M., & Showkati, H. (2012). Experimental investigation on cyclic behavior of perforated steel plate shear walls. Journal of Constructional Steel Research, 70, 308-316.
12. Paslar, N., Farzampour, A., & Hatami, F. (2020). Infill plate interconnection effects on the structural behavior of steel plate shear walls. Thin-Walled Structures, 149, 106621.
13. Mirsadeghi, M. R. H., & Fanaie, N. (2021). Steel plate shear walls with partial length connection to vertical boundary element. Structures, 33, [page range].
14. Jiang, Z. Q., Wang, J. J., Shen, C. J., Yan, T., & Su, L. (2024). Cyclic loading behavior of novel internally stiffened double steel plate shear wall. *Journal of Building Engineering*, *90*, 109462.
15. Wen, C. B., Sun, H. J., Liu, Y. Z., Hou, Y. G., Zuo, J. Q., & Guo, Y. L. (2024). Cyclic tests and shear resistance design of stiffened corrugated steel plate shear walls. *Engineering Structures*, *298*, 117060.
16. Kordzangeneh, G., Rezaeian, A., Showkati, H., Yekrangnia, M., & Dehdashti, S. A. H. (2021, October). Experimental study on the effect of square opening size and location on cyclic response of steel plate shear walls. In *Structures* (Vol. 33, pp. 4655-4669). Elsevier.
17. Feng, X. T., Yu, J. G., Carvelli, V., & Guo, H. C. (2024). Wall-frame interaction of steel plate shear wall strengthened by foam-infilled corrugated CFRP panel. *Journal of Building Engineering*, *94*, 109900.
18. Paslar, N., Farzampour, A., Soltanpour Khazaei, S., Chalangaran, N., & Hu, J. W. (2025). Enhancing the performance of steel plate shear walls with partially connected infill plates. *Journal of Building Pathology and Rehabilitation*, *10*(2), 125.
19. Zhong, H., Jie, C., Hou, J., Hang, X., Li, C., & Guo, L. (2025). Cyclic experiments and design of partially buckling-restrained steel plate shear walls with vertical bolted restrainers. *Thin-Walled Structures*, 113623.
20. Li, S., Hao, J., Tian, W., & Wu, X. (2025). Experimental and numerical investigation of coupled steel plate shear wall with slits. *Journal of Constructional Steel Research*, *230*, 109526.
21. Razavi, M., & Bhowmick, A. K. (2025, August). Collapse risk and seismic loss assessment of self-centering steel plate shear walls with circular perforations. In *Structures* (Vol. 78, p. 109334). Elsevier.
22. Dassault Systèmes. (2012). ABAQUS 6.12.1 analysis user's manual.

23. Building Seismic Safety Council. (1997). NEHRP guidelines for the seismic rehabilitation of buildings (FEMA 273). Federal Emergency Management Agency.